

Measuring the Higgs boson mass with transverse mass variables

Kiwoon Choi^a, Jae Sik Lee^b, and Chan Beom Park^a

^a*Department of Physics, KAIST, Daejeon 305-701, Korea*

^b*Physics Division, National Center for Theoretical Sciences, Hsinchu, Taiwan*

ABSTRACT

We provide a comparative study of the Higgs boson mass measurements based on two approaches to the dileptonic decay of W bosons produced by the Higgs boson decay, one using the kinematic variable M_T^{true} and the other using the M_{T2} -assisted on-shell reconstruction of the invisible neutrino momenta. We find that these two approaches can determine the Higgs boson mass with a similar accuracy for both of the two main production mechanisms of the SM Higgs boson at the LHC, i.e. the gluon-gluon fusion and the weak vector boson fusion. We also notice that the Higgs signal distribution for the gluon-gluon fusion becomes narrower under the M_{T2} cut, while the corresponding background distribution becomes flatter, indicating that one might be able to reduce the systematic uncertainties of mass measurement with an appropriate M_{T2} cut.

1 Introduction

The utmost target of the LHC is to discover the Higgs boson and study its fundamental properties to establish the mechanism of electroweak symmetry breaking as the origin of particle masses [1,2]. The unsuccessful search at the LEP experiment set a lower bound on the standard model (SM) Higgs mass at 114.4 GeV (95 % C.L.) [3], while the analysis of the electroweak precision data indicates a relatively light SM Higgs boson with $m_H \lesssim 185$ GeV at the 95 % confidence level [4]. Combined with the recent Tevatron search excluding $158 \text{ GeV} \leq m_H \leq 175 \text{ GeV}$ [5], we anticipate that the SM Higgs boson most probably lies in the mass range between 114.4 GeV and 158 GeV.

At the LHC, the Higgs boson is mainly produced by the gluon-gluon fusion (GGF) mechanism, and the second most important source is the weak vector boson fusion (VBF) process [6,7]. While the production cross section of GGF is about 10 times larger than that of VBF for the Higgs mass region $114.4 \text{ GeV} \leq m_H \leq 170 \text{ GeV}$, VBF has its advantage in a kinematic structure containing two forwarding tagging jets with a large rapidity gap, which can be exploited to isolate the Higgs boson signal from backgrounds and to study the signal properties [8–10].

The specific search strategy of the Higgs boson at the LHC depends on its mass and decay pattern. According to the combined study on the expected Higgs discovery significance at ATLAS with 10 fb^{-1} luminosity [1], when the Higgs boson is lighter than 130 GeV, the main search channel is GGF with the Higgs boson decaying into two tau leptons or into two photons. On the other hand, for $130 \text{ GeV} \lesssim m_H \lesssim 150 \text{ GeV}$, the following three channels are available with a similar significance: (i) GGF with the Higgs boson decaying into two Z bosons which subsequently decay into four charged leptons, (ii) GGF with the Higgs boson decaying into two W bosons, which subsequently decay into two charged leptons and two neutrinos, and (iii) VBF with the Higgs boson decaying into two W bosons, which subsequently decay into two charged leptons and two neutrinos. Finally, for $150 \text{ GeV} \lesssim m_H \lesssim 190 \text{ GeV}$, Higgs boson decay into two Z bosons is relatively suppressed, while channels (ii) and (iii) remain as the dominant search channels [11]. Therefore, dileptonic W boson decays play a crucial role in the Higgs boson search at the LHC when the Higgs boson weighs between 130 GeV and 190 GeV. Furthermore, if one can improve the efficiency of dileptonic channels, they might play an important role even for m_H lighter than 130 GeV.

In dileptonic W boson decays, there are two invisible neutrinos which make a direct reconstruction of the Higgs boson mass impossible. To overcome this difficulty, one can consider various kind of transverse mass variables.* A well-known example is the transverse

*The general concept of transverse mass has been introduced and studied as early as in Ref. [12]. In our work, we concentrate on the recently proposed transverse mass variables such as M_T^{true} , M_{T2} , and m_H^{maos} .

mass of a W boson pair in the process $H \rightarrow WW \rightarrow \ell\nu\ell'\nu'$ ($\ell, \ell' = e, \mu$ and $\nu, \nu' = \nu_e, \nu_\mu$):

$$M_T^2(WW) = m_{\ell\ell'}^2 + m_{\nu\nu'}^2 + 2 \left(\sqrt{|\mathbf{p}_T^{\ell\ell'}|^2 + m_{\ell\ell'}^2} \sqrt{|\mathbf{p}_T^{\nu\nu'}|^2 + m_{\nu\nu'}^2} - \mathbf{p}_T^{\ell\ell'} \cdot \mathbf{p}_T^{\nu\nu'} \right), \quad (1)$$

where m_X and \mathbf{p}_T^X denote the invariant mass and the transverse momentum, respectively, of $X = \ell\ell', \nu\nu'$. Obviously $M_T(WW)$ is bounded by m_H , and this upper bound is saturated when $\ell\ell'$ and $\nu\nu'$ have the same rapidity, $\eta_{\ell\ell'} = \eta_{\nu\nu'}$, where $\eta = \frac{1}{2} \ln(E + p_L)/(E - p_L)$ for the longitudinal momentum p_L . Therefore, if $M_T(WW)$ is correctly reconstructed event by event, the Higgs boson mass can be read off from the endpoint value of $M_T(WW)$ distribution. However, there is an obstacle to this approach: $m_{\nu\nu'}$ cannot be experimentally determined, although $\mathbf{p}_T^{\nu\nu'}$ can be deduced from the missing transverse momentum of the event. One way to bypass this difficulty is to simply take $m_{\nu\nu'} = m_{\ell\ell'}$ [13], and consider the distribution of

$$M_T^{\text{approx}} \equiv M_T(WW)|_{m_{\nu\nu'}=m_{\ell\ell'}}, \quad (2)$$

which would provide a good approximation to the true value of $M_T(WW)$ if the W boson pair were produced at near-threshold. However, in reality, a sizable number of events are not close to such a threshold, and as a result, M_T^{approx} is not bounded by m_H anymore. Still, the detailed shape of its distribution has a certain correlation with m_H , so M_T^{approx} has been widely used in the previous studies of the Higgs boson search and mass measurement [1, 8, 10].

Recently, it has been noticed that an alternative transverse mass variable [14],

$$M_T^{\text{true}} \equiv M_T(WW)|_{m_{\nu\nu'}=0}, \quad (3)$$

may determine the Higgs boson mass more accurately than M_T^{approx} does, since it is bounded by m_H and thus could have a stronger correlation with m_H [14, 15]. Obviously, for each event

$$M_T^{\text{true}} \leq M_T(WW) \leq m_H, \quad (4)$$

and the upper bound of M_T^{true} is saturated by the events with $\eta_{\ell\ell'} = \eta_{\nu\nu'}$ and $m_{\nu\nu'} = 0$; therefore, the endpoint value of M_T^{true} distribution indeed corresponds to m_H .

There is another widely discussed transverse mass variable, M_{T2} , which is defined for a generic event with two identical invisible particles [16] and was applied recently to the mass measurement of supersymmetric particles [16, 17]. For the Higgs boson event $H \rightarrow WW \rightarrow \ell(p)\nu(k)\ell'(q)\nu'(l)$, M_{T2} is given by

$$M_{T2} \equiv \min_{\mathbf{k}_T + \mathbf{l}_T = \mathbf{p}_T} \left[\max \left\{ M_T^{(1)}, M_T^{(2)} \right\} \right], \quad (5)$$

where $M_T^{(1)}$ and $M_T^{(2)}$ are the transverse masses of the two leptonically decaying W bosons:

$$\left(M_T^{(1)} \right)^2 = 2 \left(|\mathbf{p}_T| |\mathbf{k}_T| - \mathbf{p}_T \cdot \mathbf{k}_T \right), \quad \left(M_T^{(2)} \right)^2 = 2 \left(|\mathbf{q}_T| |\mathbf{l}_T| - \mathbf{q}_T \cdot \mathbf{l}_T \right). \quad (6)$$

This M_{T2} has an endpoint at $m_H/2$ when $m_H \leq 2m_W$ [18], suggesting that M_{T2} also might be useful for the Higgs boson mass measurement.

In fact, with M_{T2} and additional on-shell constraints, one can approximately reconstruct the invisible particle 4-momenta in each event [19]. This method of “ M_{T2} -assisted-on-shell (MAOS) reconstruction” of invisible particle momenta has been applied to the Higgs boson event $H \rightarrow WW \rightarrow \ell(p)\nu(k)\ell'(q)\nu'(l)$ [18] in order to examine the invariant mass variable

$$(m_H^{\text{maos}})^2 \equiv (p + q + k^{\text{maos}} + l^{\text{maos}})^2, \quad (7)$$

where k^{maos} and l^{maos} are the reconstructed neutrino 4-momenta. It was then argued that the distribution of this MAOS Higgs mass exhibits a peak at the true Higgs boson mass. Furthermore, the reconstructed MAOS momenta k^{maos} and l^{maos} are closer to the true neutrino momenta for the events near the upper endpoint of M_{T2} . As a result, the m_H^{maos} distribution can exhibit even a narrow resonance peak at m_H when a strong M_{T2} cut is employed. These observations suggest that m_H^{maos} might provide a powerful tool to probe the Higgs boson mass through dileptonic W boson decays.

Since it has been claimed that various kinematic variables are useful for the Higgs boson mass measurement, it would be instructive to perform a comparative study of the efficiencies of those variables in the LHC environment. In this paper, we wish to perform such a comparative study for M_T^{true} , M_{T2} , and m_H^{maos} , and explore the possibility to improve the efficiency of the analysis. This paper is organized as follows. In Sec. 2, we discuss the distinctive features of M_T^{true} , M_{T2} , and m_H^{maos} for dileptonic W boson decays, mainly focusing on the possible correlations between these three kinematic variables. From the discussion in Sec. 2, it is evident that M_{T2} is less efficient than M_T^{true} as a main observable for the Higgs boson search. However, M_{T2} might be a useful cut variable in the analysis using M_T^{true} or m_H^{maos} as the main observable. As for the comparison of M_T^{true} and m_H^{maos} , it is not obvious which one is more efficient since each variable has its own virtue and weak point. We thus perform in Secs. 3 and 4 a detailed comparative study of M_T^{true} and m_H^{maos} . Our results show that m_H^{maos} and M_T^{true} will eventually have a similar efficiency for both the GGF and VBF Higgs productions at the LHC. In this study, we also examine the possible role of M_{T2} as a cut variable, and find that the Higgs signal distribution for the GGF channel becomes narrower under the M_{T2} cut, while the background distribution becomes flatter. Although an estimate of any systematic uncertainty is beyond the scope of this paper, such behavior of the signal/background distributions under the M_{T2} cut indicates that one might be able to reduce the systematic errors in the GGF channel with an appropriate M_{T2} cut. We summarize our conclusions in Sec. 5.

2 Distinctive features of the transverse mass variables

Unlike the Higgs boson decay into two photons or two tau leptons[†], the Higgs boson mass cannot be reconstructed in the event $H \rightarrow WW^{(*)} \rightarrow \ell(p)\nu(k)\ell'(q)\nu'(l)$ due to the missing neutrinos. One then often considers the transverse mass of the W pair, $M_T(WW)$, defined in Eq. (1), as the main observable to probe the Higgs signal event [1, 8, 13, 14]. If one could determine the correct value of $m_{\nu\nu'}$ event by event, the resulting distribution of $M_T(WW)$ would have an upper endpoint at m_H . However, $m_{\nu\nu'}$ is not available, in general, and there have been two proposals to fix the unknown $m_{\nu\nu'}$. The first one is to choose $m_{\nu\nu'} = m_{\ell\ell'}$ [1, 8, 13], and consider the distribution of

$$M_T^{\text{approx}} \equiv M_T(WW)|_{m_{\nu\nu'}=m_{\ell\ell'}}. \quad (8)$$

This has been motivated by the observation that, for a Higgs boson mass close to $2m_W$, the W bosons are produced at near-threshold and almost at rest in their center-of-mass frame, for which $m_{\nu\nu'}^{\text{true}} = m_{\ell\ell'}$, where $m_{\nu\nu'}^{\text{true}}$ is the true value of $m_{\nu\nu'}$ in the event. Although this threshold approximation is not necessarily suitable for generic events and therefore M_T^{approx} is not strictly bounded from above by m_H , still the shape and range of its distribution can provide information on the Higgs boson mass. The second proposal [14] is deduced from the simple relation

$$M_T^{\text{true}} \equiv M_T(WW)|_{m_{\nu\nu'}=0} \leq M_T(WW)|_{m_{\nu\nu'}=m_{\nu\nu'}^{\text{true}}} \leq m_H. \quad (9)$$

It was reported that one can obtain a more accurate Higgs boson mass by using M_T^{true} rather than using M_T^{approx} [14, 15].

For the event $H \rightarrow WW^{(*)} \rightarrow \ell(p)\nu(k)\ell'(q)\nu'(l)$, one may exploit the event variable M_{T2} which has been designed for a general situation with two invisible particles (with the same mass) in the final state [16]. The variable is defined as

$$M_{T2} \equiv \min_{\mathbf{k}_T + \mathbf{l}_T = \mathbf{p}_T} \left[\max \left\{ M_T^{(1)}, M_T^{(2)} \right\} \right], \quad (10)$$

where $M_T^{(1)}$ and $M_T^{(2)}$ are the transverse masses of the two leptonically decaying W bosons:

$$\left(M_T^{(1)} \right)^2 = 2 \left(|\mathbf{p}_T| |\mathbf{k}_T| - \mathbf{p}_T \cdot \mathbf{k}_T \right), \quad \left(M_T^{(2)} \right)^2 = 2 \left(|\mathbf{q}_T| |\mathbf{l}_T| - \mathbf{q}_T \cdot \mathbf{l}_T \right). \quad (11)$$

For a specific set of events for which the Higgs boson has vanishing transverse momentum, $\mathbf{p}_T = -\mathbf{p}_T - \mathbf{q}_T$, one can use the following analytic expression of M_{T2} :

$$M_{T2}^2 = 2 \left(|\mathbf{p}_T| |\mathbf{q}_T| + \mathbf{p}_T \cdot \mathbf{q}_T \right) \quad (12)$$

[†] In the di-tau channel, each tau decays to hadron (or lepton) + a neutrino(s). Although the final state neutrinos make a full reconstruction of the event impossible, it is known that the di-tau invariant mass can be determined well in collinear approximation [20].

to find the upper bound

$$M_{T2}^2 \leq (|\mathbf{p}_T| + |\mathbf{q}_T|)^2 \leq \frac{m_H^2}{4}. \quad (13)$$

Although the above relation is derived for the specific event set with vanishing Higgs transverse momentum, it is likely that the same upper bound applies for generic Higgs boson events with nonvanishing Higgs boson transverse momentum. We found through numerical analysis that it is indeed the case and the inequality $M_{T2} \leq m_H/2$ remains true for generic dileptonic Higgs boson events $H \rightarrow WW^{(*)} \rightarrow \ell\nu\ell'\nu'$. [See the later discussion of the inequality between M_{T2} and M_T^{true} in Eq. (21).] On the other hand, in the case that both W bosons are on shell, M_{T2} is bounded by m_W . Combining this with (13), one may find that the M_{T2} of the Higgs boson decay is bounded by [18]

$$M_{T2}^{\text{max}} = \begin{cases} m_H/2 & \text{for } m_H \leq 2m_W \\ m_W & \text{for } m_H \geq 2m_W, \end{cases} \quad (14)$$

implying that M_{T2} can provide information on the Higgs boson mass through its endpoint.

Apart from M_T^{approx} , M_T^{true} , and M_{T2} in dileptonic W boson decays, there has been a proposal to reconstruct an invariant mass by using the MAOS reconstruction of the two neutrino momenta [18]. In MAOS reconstruction, the transverse momenta are defined as the ones that determine the value of M_{T2} , i.e.

$$M_{T2}(\mathbf{p}_T, \mathbf{q}_T, \mathbf{p}'_T) = M_T^{(1)}(\mathbf{p}_T, \mathbf{k}_T^{\text{maos}}) = M_T^{(2)}(\mathbf{q}_T, \mathbf{l}_T^{\text{maos}} = \mathbf{p}'_T - \mathbf{k}_T^{\text{maos}}), \quad (15)$$

while the longitudinal and energy components are obtained from the following constraints[‡]:

$$(k^{\text{maos}})^2 = (l^{\text{maos}})^2 = 0, \quad (p + k^{\text{maos}})^2 = (q + l^{\text{maos}})^2 = M_{T2}^2. \quad (16)$$

It was noticed that the MAOS 4-momenta determined as the solutions of (15) and (16) provide a reasonable approximation to the true neutrino 4-momenta, and they become closer to the true momenta for the near-endpoint events in the M_{T2} distribution [18, 19]. Then the distribution of the following invariant mass (\equiv MAOS Higgs boson mass),

$$(m_H^{\text{maos}})^2 \equiv (p + q + k^{\text{maos}} + l^{\text{maos}})^2 \quad (17)$$

exhibits a peak at the true Higgs boson mass, and the peak shape becomes narrower if one imposes an event cut selecting the events near the endpoint of M_{T2} . Although such an M_{T2} cut can cause the m_H^{maos} distribution to have a resonance peak at m_H and also might eliminate some of the backgrounds, it can also sacrifice the number of the Higgs

[‡]Note that one could use m_W instead of M_{T2} in the second constraints if both of the W bosons are on shell. Our scheme to use M_{T2} can be applicable irrespective of whether the W bosons are on shell or off shell.

signal, thus worsening the statistical significance of the mass measurement. Therefore for a given luminosity a careful analysis is required to see if the efficiency of the Higgs mass measurement can be improved by a proper M_{T2} cut.

To proceed, let us consider a specific set of events for which the W boson pair has a small transverse momentum: $\mathbf{p}_T^{WW} \approx 0$. Although it does not cover the full event set, this subset of events reveal some of the essential features of the kinematic variables under discussion. For those events with small \mathbf{p}_T^{WW} , we have

$$\not{\mathbf{p}}_T = -(\mathbf{p}_T + \mathbf{q}_T),$$

and then the following simple expressions of M_{T2} and MAOS momenta are available [18,19]:

$$\begin{aligned} \mathbf{k}_T^{\text{maos}} &= -\mathbf{q}_T, & k_L^{\text{maos}} &= \frac{|\mathbf{k}_T^{\text{maos}}|}{|\mathbf{p}_T|} p_L, \\ \mathbf{l}_T^{\text{maos}} &= -\mathbf{p}_T, & l_L^{\text{maos}} &= \frac{|\mathbf{l}_T^{\text{maos}}|}{|\mathbf{q}_T|} q_L, \\ M_{T2}^2 &= 2(|\mathbf{p}_T||\mathbf{q}_T| + \mathbf{p}_T \cdot \mathbf{q}_T). \end{aligned} \quad (18)$$

With these expressions of M_{T2} and MAOS momenta, it is straightforward to find

$$\begin{aligned} (m_H^{\text{maos}})^2 &= \left(2 + \left| \frac{\mathbf{p}_T}{\mathbf{q}_T} \right| + \left| \frac{\mathbf{q}_T}{\mathbf{p}_T} \right| \right) \left(2(|\mathbf{p}_T||\mathbf{q}_T| + \mathbf{p}_T \cdot \mathbf{q}_T) + m_{\ell\ell'}^2\right), \\ M_T^{\text{true}} &= |\mathbf{p}_T + \mathbf{q}_T| + \sqrt{|\mathbf{p}_T + \mathbf{q}_T|^2 + m_{\ell\ell'}^2}. \end{aligned} \quad (19)$$

Since

$$\begin{aligned} M_{T2}^2 &= 2(|\mathbf{p}_T||\mathbf{q}_T| + \mathbf{p}_T \cdot \mathbf{q}_T) \leq |\mathbf{p}_T + \mathbf{q}_T|^2, \\ m_{\ell\ell'}^2 &= 2(|\mathbf{p}| |\mathbf{q}| - \mathbf{p} \cdot \mathbf{q}) \geq 0, \end{aligned} \quad (20)$$

both m_H^{maos} and M_T^{true} are bounded below by $2M_{T2}$, and therefore

$$2M_{T2} \leq M_T^{\text{true}} \leq m_H, \quad 2M_{T2} \leq m_H^{\text{maos}}. \quad (21)$$

Although the above inequalities between M_{T2} , M_T^{true} and m_H^{maos} could be derived analytically only for the events with $\mathbf{p}_T^{WW} = 0$, we find numerically that they hold true also for the events with $\mathbf{p}_T^{WW} \neq 0$. In Fig. 1 (left panel), we show the distributions of these three kinematic variables for the true Higgs mass $m_H = 160$ GeV. Here we use the Higgs boson events produced by the GGF process at the LHC, while incorporating the detector effects with the fast detector simulation program PGS4 [21]. Figure 1 (left panel) shows, first of all, that both M_T^{true} and $2M_{T2}$ have a common upper endpoint at $m_H = 160$ GeV, as we have anticipated in the above discussion. However, the M_T^{true} distribution is significantly narrower than the $2M_{T2}$ distribution, as implied by the first inequality in Eq. (21). This

indicates that M_T^{true} is more sensitive to m_H than M_{T2} , and thus is a more efficient variable to determine m_H . If one compares M_T^{true} to m_H^{maos} , Fig. 1 (left panel) shows that m_H^{maos} has a peak at m_H , while M_T^{true} has an endpoint at m_H . With this feature, one might expect that m_H^{maos} is more sensitive to m_H than M_T^{true} . However the M_T^{true} distribution around m_H is significantly narrower than the m_H^{maos} distribution, and thus one needs a detailed analysis to see which of M_T^{true} and m_H^{maos} is more efficient for the determination of m_H . In the next two sections, we perform such an analysis for both the GGF Higgs production (Sec. 3) and the VBF Higgs production (Sec. 4) at the LHC.

3 Measuring the Higgs boson mass in GGF

In this section, we consider the SM Higgs boson production at the LHC through the GGF process and its decay into two leptonically decaying W bosons. To investigate the experimental performance of m_H^{maos} and M_T^{true} , we use the PYTHIA6.4 event generator [22] at the proton-proton center-of-mass energy of 14 TeV. The generated events have been further processed through the fast detector simulation program PGS4 [21] to incorporate the detector effects with reasonable efficiencies and fake rates. The dominant background comes from the continuum $q\bar{q}, gg \rightarrow WW \rightarrow l\nu l'\nu'$ process, and we also include the $t\bar{t}$ background in which the two top quarks decay into a pair of W bosons and two b jets. For the details of the MC event samples of the SM Higgs boson signal and the two main backgrounds, and also the employed event selection cuts, we refer to Ref. [18].

In Fig. 1, we show the m_H^{maos} and M_T^{true} distributions of the signal events for $m_H = 160$ GeV without (left panel) and with (right panel) the M_{T2} cut: $M_{T2} > (M_{T2})^{\text{cut}} = 60$ GeV. We use the same event samples at the detector level as in Ref. [18] but do not apply the event selection cuts other than the M_{T2} cut. First we note that the M_T^{true} distribution is bounded above by $m_H = 160$ GeV, while the m_H^{maos} distribution is peaked around it, as noticed in the discussion of the previous section. Under an M_{T2} cut, both distributions are bounded from below by $2(M_{T2})^{\text{cut}} = 120$ GeV with a rather good approximation, which can be understood by the inequalities in (21). Incidentally, in the m_H^{maos} distribution, the region above m_H is less sensitive to the M_{T2} cut than the region below m_H . We also see clearly that the M_T^{true} distribution is narrower than the m_H^{maos} distribution as implied by Eq. (21).

Next, we proceed to perform the template likelihood fitting to the M_T^{true} and m_H^{maos} distributions. Here, a template means a simulated distribution with a trial Higgs mass which, in general, is different from the nominal one used to generate the data. For each pseudoexperiment distribution with the nominal Higgs mass m_H , 11 templates are generated with the trial Higgs masses between $m_H - 10$ GeV and $m_H + 10$ GeV, in steps of 2 GeV. For example, in each frame of Fig. 2, the solid line shows the template distribution

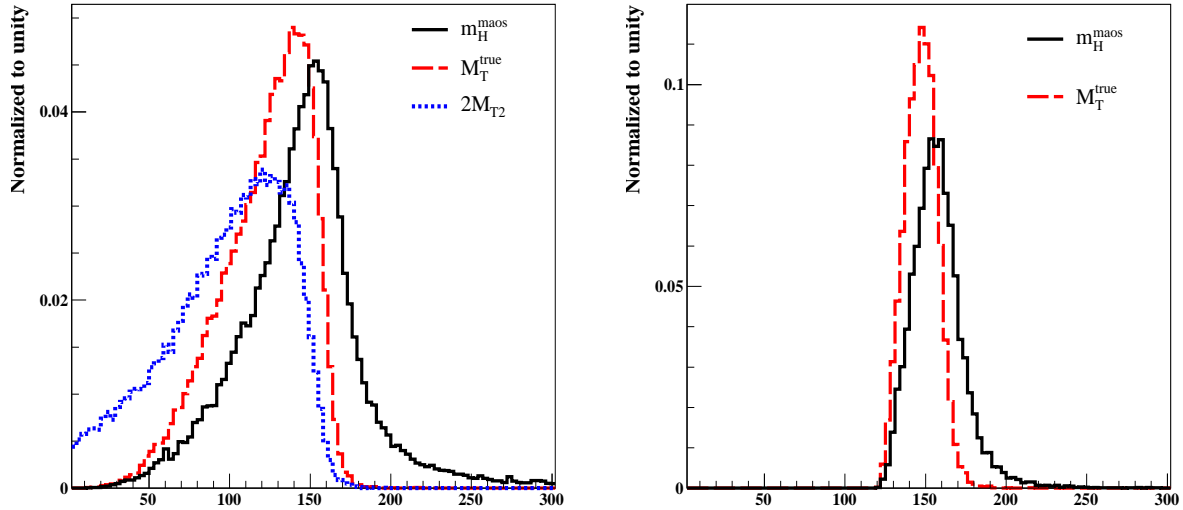


Figure 1: The signal m_H^{maos} (black solid line) and M_T^{true} (red dashed line) distributions at the detector-level without (left panel) and with (right panel) the M_{T2} cut, $M_{T2} > 60$ GeV. The Higgs boson mass is taken to be 160 GeV, and we use the same event samples as in Ref. [18].

when the trial Higgs mass is the same as the nominal one. Each template is normalized to the corresponding pseudoexperiment distribution. For the definitions of the likelihood between a pseudoexperiment data distribution and a template, and also for more on the Higgs masses and $1\text{-}\sigma$ errors obtained by fitting the log likelihood distributions, we again refer to Ref. [18].

Empirically, the template likelihood fitting, which is used to estimate the efficiency of the Higgs mass determination in this work, provides a better result when the width of the distribution is narrower. On the other hand, compared to the peak of the distribution which is generally easier to determine, the endpoints are more vulnerable to detector smearing, backgrounds and low statistics. Even though the peak of the M_T^{true} distribution does not have a strong correlation with the input Higgs mass like that of the m_H^{maos} distribution, the overall shape has a definite correlation with the Higgs boson mass and, moreover, its narrower width might result in a comparable sensitivity to m_H^{maos} . The problem is the shape of the background distribution which could smear the edge structure of M_T^{true} . In Fig. 2, we have shown the m_H^{maos} (left panels) and M_T^{true} (right panels) distributions for the Higgs signal and the backgrounds. We use the same detector-level event samples as in Ref. [18], and all the event selection cuts are applied.

Our MC study shows that, generically, the background distributions for both M_T^{true}

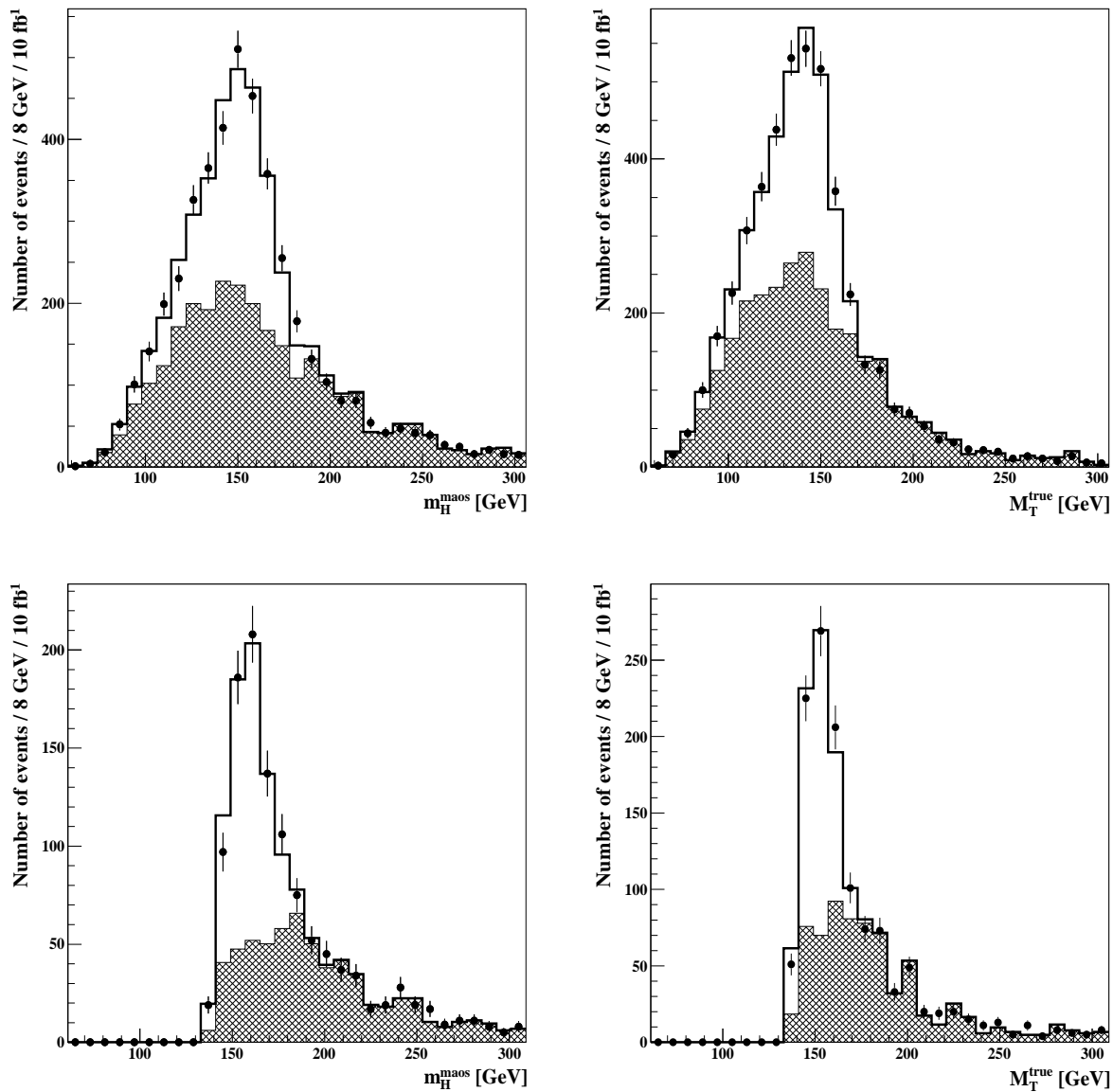


Figure 2: The m_H^{maos} (left frames) and the M_T^{true} (right frames) distributions at 10 fb^{-1} luminosity. In each frame, the shaded region represents the backgrounds ($t\bar{t}$ and WW) and the event selection cuts without (upper frames) and with (lower frames) the M_{T2} cut ($M_{T2} > 66 \text{ GeV}$) imposed. The Higgs boson mass is taken to be 160 GeV , and we again refer to Ref. [18] for the details.

and m_H^{maos} become flatter if we impose a stronger M_{T2} cut. On the other hand, a stronger M_{T2} cut causes the signal distributions to have a narrower shape (see Fig. 1). This behavior of the signal and background under the M_{T2} cut suggests that one might be able to improve

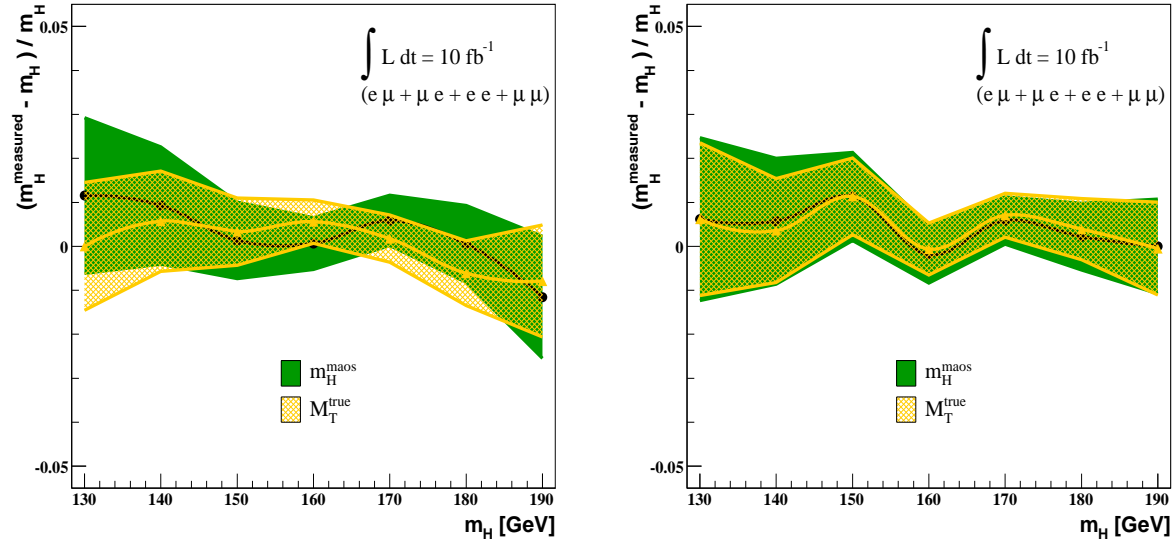


Figure 3: The bands showing the $1\text{-}\sigma$ deviation of the statistical error for the Higgs boson mass determined by the m_H^{maos} and M_T^{true} distributions in the GGF process $gg \rightarrow H \rightarrow WW^{(*)} \rightarrow l\nu l'\nu'$. The dots and lines denote the Higgs boson mass obtained by the likelihood fit to the distributions. We use the same event sample and the cut procedure as in Ref. [18], where the right (left) panel is the result with (without) an optimal M_{T2} cut, chosen differently for different values of m_H .

the efficiency of the Higgs mass measurement with an appropriate M_{T2} cut, particularly reduce the systematic uncertainties associated with various origins such as the detector energy resolution, fit routines and poorly estimated backgrounds. As for statistical error, one needs a detailed analysis, as the improvement due to better shapes of signal and background distributions can be compensated by the reduced statistics. Indeed, for an integrated luminosity $\sim 10 \text{ fb}^{-1}$, we find (Fig. 3) that there is no appreciable improvement of the statistical error gained by the M_{T2} cut, although the situation might be different at higher luminosity.

In Fig. 3, we show the Higgs boson masses and the $1\text{-}\sigma$ (statistical) errors obtained by the likelihood fit to the m_H^{maos} and M_T^{true} distributions in the GGF process $gg \rightarrow H \rightarrow WW^{(*)} \rightarrow l\nu l'\nu'$. We see that the reconstructed mass is rather close to the input one. For the sake of comparison, we have not employed an M_{T2} cut in the left frame since the cut was not included in the original suggestion of the M_T^{true} variable [14]; however, it is employed in the right frame. We observe that the efficiency of m_H^{maos} is comparable to that of M_T^{true} up to systematic errors, which are not considered in our analysis. In particular, when the M_{T2} cut is employed, it is hard to say which one shows a better efficiency. Still, we note that m_H^{maos} could be a better choice when the distribution is spoiled by some unknown

backgrounds beyond the SM, since the peak is less vulnerable to unknown backgrounds than the endpoint.

4 Measuring the Higgs boson mass in VBF

In this section, we turn to the VBF process, which is the second most important production channel of the SM Higgs boson at the LHC. The characteristic feature of the process is the existence of the two forward tagging jets with suppressed hadronic activity between them and the central Higgs decay products. Thanks to the exchanges of the colorless vector bosons in the process, these features lead to a fairly clean environment with well-isolated signal events in a low background. Therefore, the VBF process is useful to measure properties of the Higgs boson in a hadron collider environment.

The same variables introduced in the GGF process could be used to determine the Higgs boson mass in VBF, since the tagging jets provide additional information without touching the decay of the Higgs boson itself. To investigate the experimental performance of the MAOS Higgs mass at the LHC through the VBF process, we have generated MC event samples of the signal $H + 2j$ events and the main $t\bar{t}$ background events by `PYTHIA6.4` [22]. The subleading background, i.e. electroweak $WW + 2j$ event showing a similar characteristic, has been generated using `MadGraph/MadEvent` [23]. The generated events have been further processed with the fast detector simulation program `PGS4` [21], which approximates an ATLAS or CMS-like detector. The `PGS4` program uses a cone algorithm for jet reconstruction, with a default value of the cone size $\Delta R = 0.5$, where ΔR is a separation in the azimuthal angle and pseudorapidity plane[§]. We note that the b -jet tagging efficiency is introduced as a function of the jet transverse energy and pseudorapidity, with a typical value of about 50 % in the central region for the high energy jets.

Proceeding in a similar way as in Ref. [8], we have imposed the following basic selection cuts on the Higgs signal and the backgrounds:

- Preselection cuts
- b -jet veto
- Tag-jet conditions (forward jet tagging, leptons between jets, central jet veto)
- $\gamma^*/Z +$ jets, $Z \rightarrow \tau\tau$ rejection

[§]The pseudorapidity is defined as $\eta = -\ln \tan(\theta/2)$ for the angle θ between the particle momentum and the beam axis. Note that the pseudorapidity for a massless particle is equal to the rapidity defined as $\eta = \frac{1}{2} \ln(E + p_L)/(E - p_L)$.

Since the final state consists of two hard jets, two charged leptons and significant missing transverse energy, the preselection cuts should be the minimal conditions to be imposed. Specifically, we require at least two jets with $p_T > 20$ GeV and $|\eta| < 4.8$, and two isolated, opposite-sign leptons (e or μ) with $p_T > 15$ GeV, and $|\not{p}_T| > 30$ GeV. The b -jet veto is used to exclude the main $t\bar{t}$ background which contains two b jets. The tag-jet conditions should reflect the characteristic features of the VBF process: two forward tagging jets with suppressed hadronic activity between them and central Higgs decay products. In this work, we define the tagging jets as the two highest p_T jets in the event while rejecting the event if they are in the same hemisphere. Explicitly, we have imposed the following tag-jet conditions.

- Forward jet tagging: the two hardest jets are required to be in opposite hemispheres ($\eta_{j_1} \times \eta_{j_2} < 0$) and to have a pseudorapidity separation $|\Delta\eta_{j_1 j_2}| > 3$.
- Leptons between jets: both leptons are required to be between the tag jets in pseudorapidity.
- Central jet veto: the event is rejected if it contains any extra jet (in addition to the two forward tagging jets) with $p_T > 20$ GeV in the pseudorapidity region $|\eta| < 3.2$.

The last basic selection cut is to reject the Drell-Yan background involving the variable [see Eq. (1)]:

$$m_T^{ll\nu} \equiv M_T(WW)|_{m_U=m_{\nu\nu}=0}. \quad (22)$$

Though the Drell-Yan background has been neglected in this work, we have included the rejection cut to see its effect on the signal and the other background events under consideration. For the $Z \rightarrow \tau\tau$ rejection, the di-tau invariant mass is constructed using the collinear approximation, rejecting the events with $|M_{\tau\tau} - m_Z| < 25$ GeV.

It is well known that the spin-zero nature of the Higgs boson makes two charged leptons come out in the same direction, making its opening angle in the Higgs signal smaller than that in the background; see Fig. 4. To incorporate this spin information, in addition to the basic selections, we have further required

$$\Delta\Phi_{ll} < \Delta\Phi_{ll}^{\text{cut}}, \quad \Delta\eta_{ll} < \Delta\eta_{ll}^{\text{cut}}, \quad (23)$$

where $\Delta\Phi_{ll}$ and $\Delta\eta_{ll}$ are the transverse opening angle and pseudorapidity gap between the charged leptons.

In the literature, the dilepton invariant mass M_{ll} and the dijet invariant mass M_{jj} for two tagging jets are also used for the event cut. In Fig. 5, we show the M_{ll} and M_{jj} distributions for both the Higgs signal and the $t\bar{t}$ background. As in the GGF process discussed in the previous section, one might employ M_{T2} as a cut variable in the VBF process also. In the Higgs signal with the two tagging jets and also in the main $t\bar{t}$ background with two

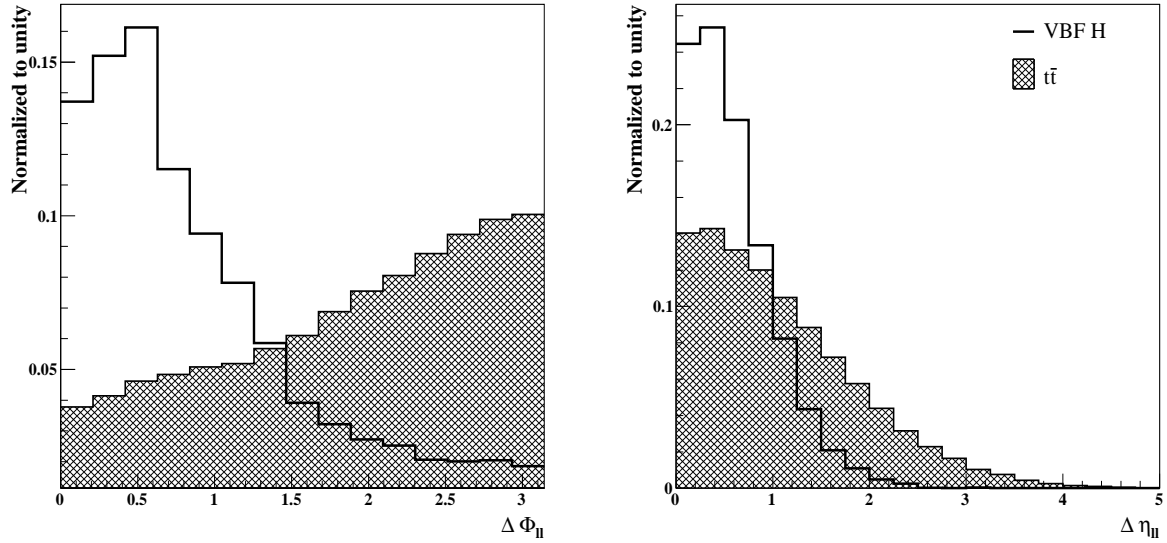


Figure 4: Transverse opening angle $\Delta\Phi_{ll}$ (left panel) and pseudorapidity gap $\Delta\eta_{ll}$ (right panel) between the charged leptons in the VBF process ($m_H = 160$ GeV) and the background events. The preselection cuts are used for the event selection.

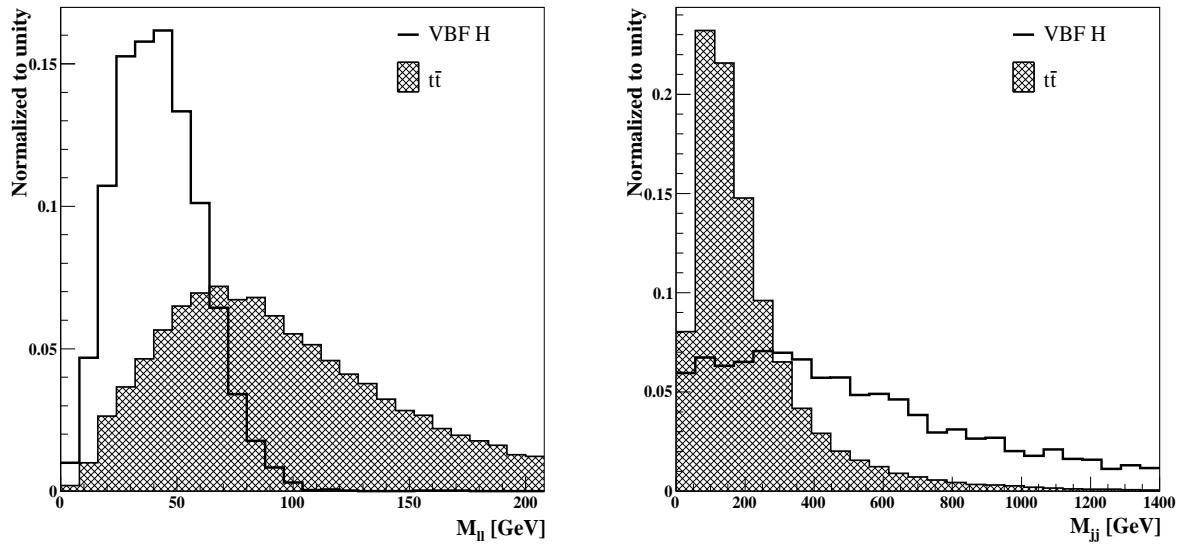


Figure 5: The M_{ll} (left panel) and M_{jj} (right panel) distributions of the signal and the $t\bar{t}$ background, after applying the preselection cuts. $m_H = 160$ GeV is taken for the signal.

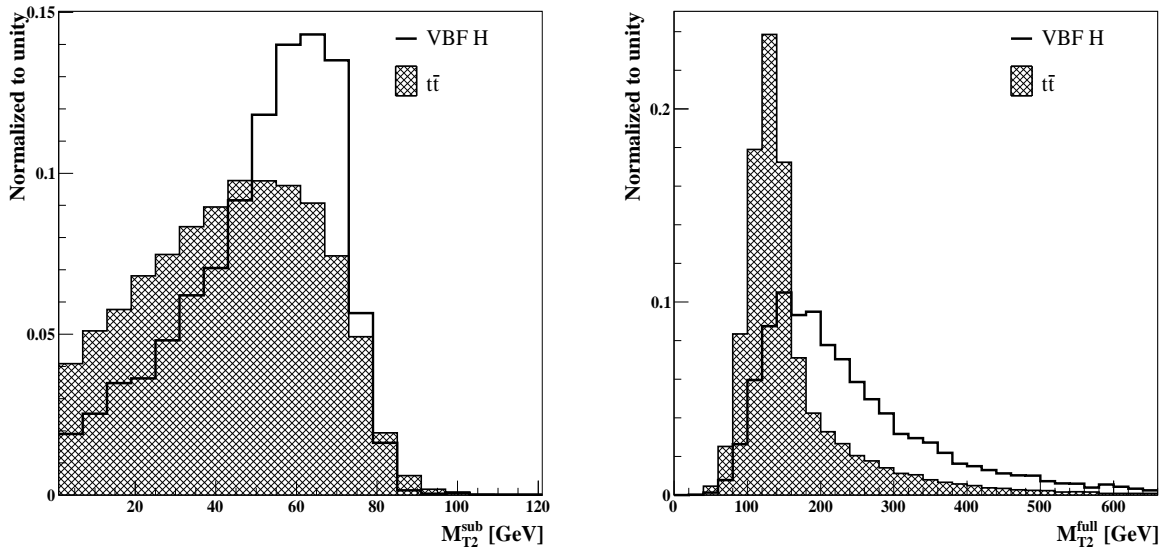


Figure 6: The M_{T2}^{sub} (left panel) and M_{T2}^{full} (right panel) distributions of the VBF process ($m_H = 160$ GeV) and the $t\bar{t}$ background, after applying the preselection cuts.

b jets, one can construct two sorts of M_{T2} —one using the transverse masses of the W -pair system and the other using the W -pair + two jets system:

$$\begin{aligned}
 M_{T2}^{\text{sub}} &\equiv \min_{\mathbf{k}_T + \mathbf{l}_T = \mathbf{p}_T} \left[\max \left\{ M_T^{\text{sub}(1)}, M_T^{\text{sub}(2)} \right\} \right], \\
 M_{T2}^{\text{full}} &\equiv \min_{\mathbf{k}_T + \mathbf{l}_T = \mathbf{p}_T} \left[\max \left\{ M_T^{\text{full}(1)}, M_T^{\text{full}(2)} \right\} \right], \quad (24)
 \end{aligned}$$

where $M_T^{\text{sub}(i)}$ and $M_T^{\text{full}(i)}$ are the transverse masses of $W^{(i)} \rightarrow l^{(i)}\nu^{(i)}$ and $j^{(i)}W^{(i)} \rightarrow j^{(i)}l^{(i)}\nu^{(i)}$, respectively. The M_{T2}^{sub} variable is defined without any combinatorial ambiguity and bounded from above by $\min(m_W, m_H/2)$ [see Eq. (14)] in the signal and by m_W in the background. On the other hand, there is a combinatorial uncertainty in constructing M_{T2}^{full} since, in each selected event, there are two possibilities in associating two jets with two charged leptons. Between the two possibilities, we choose the combination giving the smaller M_{T2}^{full} . Then, for the $t\bar{t}$ background, M_{T2}^{full} is bounded from above by m_t at parton level, which suggests that M_{T2}^{full} can be used as a cut variable to eliminate the $t\bar{t}$ backgrounds by requiring $M_{T2}^{\text{full}} > m_t$. For the Higgs signal events, tagging jets tend to have a large M_{jj} , which has been used to select the signals by requiring $M_{jj} > M_{jj}^{\text{cut}}$. In Fig. 6, we show the M_{T2}^{sub} (left panel) and M_{T2}^{full} (right panel) distributions for the signal and the $t\bar{t}$ background at detector level. In the right panel of Fig. 6, we observe that the M_{T2}^{full} distribution for $t\bar{t}$ backgrounds has a non-negligible tail above m_t , which arises from the fact that one (or both) of the tagging dijets used for the construction of M_{T2}^{full} is not the b jet from the top quark decay, but a hard jet coming from the initial state radiation or an erroneously

Table 1: Cut flows (in fb) for $m_H = 160$ GeV.

Selection cuts	VBF $H \rightarrow WW$	$t\bar{t}$	EW $WW + \text{jets}$	S/B
Preselection	33.8	10910.0	15.9	0.0031
b -jet veto	32.8	5193.1	15.5	0.0063
Forward jet tagging	22.5	542.1	6.3	0.041
Leptons between jets	20.9	347.3	5.6	0.059
Central jet veto	16.8	166.9	3.5	0.099
$m_T^{l\nu} > 30$ GeV, $Z \rightarrow \tau\tau$ rej.	15.1	138.5	2.7	0.11
$M_{ll} < 85$ GeV	14.9	62.0	0.8	0.24
$M_{jj} > 550$ GeV	9.3	8.0	0.7	1.07
$\Delta\Phi_{ll} < 1.6$, $\Delta\eta_{ll} < 1.5$	8.4	5.5	0.5	1.39
$M_{T2}^{\text{full}} > 160$ GeV	8.9	7.1	0.7	1.14
$M_{T2}^{\text{sub}} > 60$ GeV	3.6	1.7	0.3	1.80
$\Delta\Phi_{ll} < 1.6$, $\Delta\eta_{ll} < 1.5$	3.6	1.6	0.2	2.00

Table 2: Cut flows (in fb) for $m_H = 140$ GeV.

Selection cuts	VBF $H \rightarrow WW$	$t\bar{t}$	EW $WW + \text{jets}$	S/B
Preselection	17.6	10910.0	15.9	0.0016
b -jet veto	17.3	5193.1	15.5	0.0033
Forward jet tagging	12.2	542.1	6.3	0.022
Leptons between jets	11.6	347.3	5.6	0.033
Central jet veto	9.8	166.9	3.5	0.058
$m_T^{l\nu} > 30$ GeV, $Z \rightarrow \tau\tau$ rej.	8.5	138.5	2.7	0.060
$M_{ll} < 85$ GeV	8.5	62.0	0.8	0.14
$M_{jj} > 550$ GeV	5.7	8.0	0.7	0.66
$\Delta\Phi_{ll} < 1.7$, $\Delta\eta_{ll} < 1.6$	5.4	5.5	0.5	0.89
$M_{T2}^{\text{full}} > 140$ GeV	5.5	7.5	0.7	0.67
$M_{T2}^{\text{sub}} > 45$ GeV	2.1	3.7	0.5	0.50
$M_{T2}^{\text{sub}} < 72$ GeV	2.1	3.1	0.3	0.62
$\Delta\Phi_{ll} < 1.7$, $\Delta\eta_{ll} < 1.6$	2.1	2.6	0.3	0.72

reconstructed jet. With this, comparing to M_{jj} in Fig. 5, we see that M_{T2}^{full} can be as efficient as M_{jj} in discriminating the Higgs signal from the $t\bar{t}$ background. On the other hand, Figs. 6 and 5 show that both the Higgs signal and the $t\bar{t}$ background have a similar shape of M_{T2}^{sub} distribution, so M_{T2}^{sub} is not so useful as a cut variable.

Table 3: The Higgs boson masses and the $1\text{-}\sigma$ statistical errors obtained by the likelihood fit to the m_H^{maos} distributions in the VBF processes at 10 fb^{-1} .

m_H (GeV)	130	140	150	160	170	180	190
Fitted value (GeV)	132.5	140.7	150.8	161.0	170.6	183.4	188.6
$1\text{-}\sigma$ error (GeV)	7.5	7.0	4.8	3.7	3.8	6.2	6.8

With the above observations, in our event selection we have applied M_{ll} and M_{jj} cuts after the basic selection cuts:

$$M_{ll} < M_{ll}^{\text{cut}}, \quad M_{jj} > M_{jj}^{\text{cut}}. \quad (25)$$

Then, more refined M_{T2} cuts have been introduced to reduce the number of background events further. In Tables 1 and 2, we show how the cross sections of the signal and backgrounds change under each selection cut for $m_H = 160\text{ GeV}$ and 140 GeV , respectively. We note that one may also use the upper cut on the M_{T2}^{sub} when $m_H \leq 2m_W$; see the third set of cuts in Table 2. This is because the signal distribution is bounded above by $m_H/2 < m_W$ in this case. This upper cut cannot be applied when $m_H \geq 2m_W$, as the M_{T2}^{sub} distributions of both the signal and the background have an equal maximum, m_W .

In Fig. 7, we show the m_H^{maos} distributions for the two nominal values of the Higgs boson mass: $m_H = 140$ and 160 GeV . Here $(m_H^{\text{maos}})^2 = (p_1 + k_1^{\text{maos}} + p_2 + k_2^{\text{maos}})^2$ for $W^{(1)}W^{(2)} \rightarrow l^{(1)}(p_1)\nu^{(1)}(k_1)l^{(2)}(p_2)\nu^{(2)}(k_2)$, where the transverse components of k_i^{maos} ($i = 1, 2$) are those used to determine M_{T2}^{sub} , and the longitudinal and energy components are fixed by the constraints $(p_1 + k_1^{\text{maos}})^2 = (p_2 + k_2^{\text{maos}})^2 = (M_{T2}^{\text{sub}})^2$ and $(k_1^{\text{maos}})^2 = (k_2^{\text{maos}})^2 = 0$. We observe that the m_H^{maos} distribution has a clear peak at the true (nominal) Higgs mass.[¶] With the m_H^{maos} distribution constructed as above, we performed a template fitting to determine the Higgs boson mass as in Sec. 3, the GGF case. The estimated Higgs masses, together with the $1\text{-}\sigma$ errors obtained by fitting the log likelihood distributions for various Higgs masses, are listed in Table 3. The $1\text{-}\sigma$ deviated value is defined as the one that increases $-\ln \mathcal{L}$ by $1/2$ [24]. We again see that the reconstructed mass is quite close to the input Higgs boson mass.

For a comparison of the efficiency of m_H^{maos} to that of M_T^{true} , we also perform a likelihood fit of the M_T^{true} distribution with the same event sets, including the backgrounds. In Fig. 8, we show the M_T^{true} template distributions (solid lines) when the trial Higgs mass is 140 GeV (left panel) and 160 GeV (right panel). The dots with error bars represent the M_T^{true} distributions for the pseudoexperiment data with the same nominal Higgs masses.

[¶]The background bump appearing around $m_H^{\text{maos}} \gtrsim 200\text{ GeV}$ is an accidental consequence of our analysis for the VBF case. We observe that it becomes less significant like as in the GGF case for a different choice of the bin size.

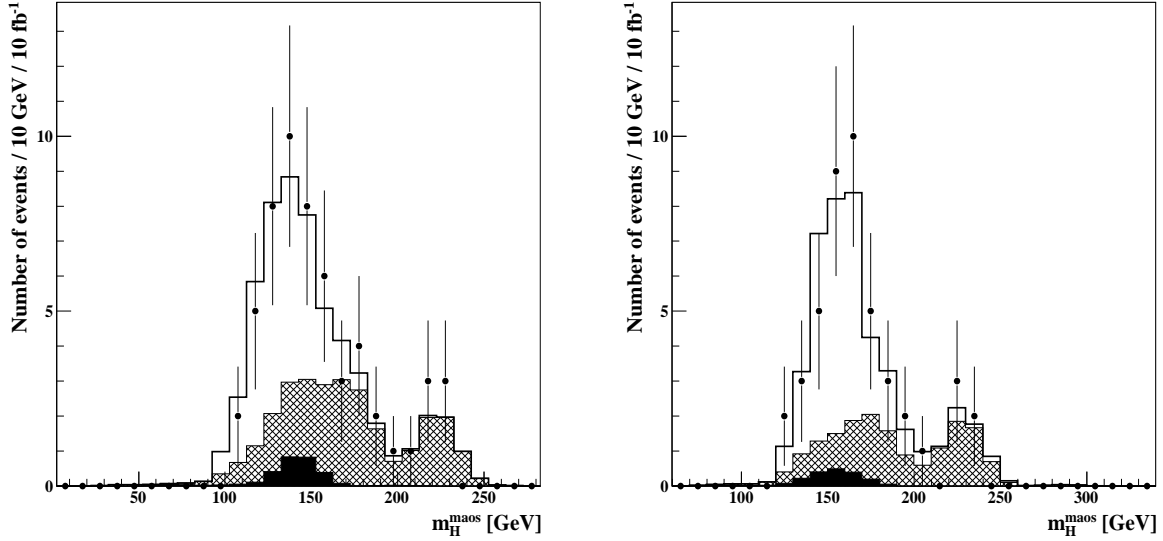


Figure 7: The m_H^{maos} distributions for the pseudoexperiment data (dots) and the template (solid line) for $m_H = 140$ (left) and 160 GeV (right) at 10 fb^{-1} . The lightly and thickly shaded regions represent the $t\bar{t}$ and $WW + 2j$ backgrounds, respectively.

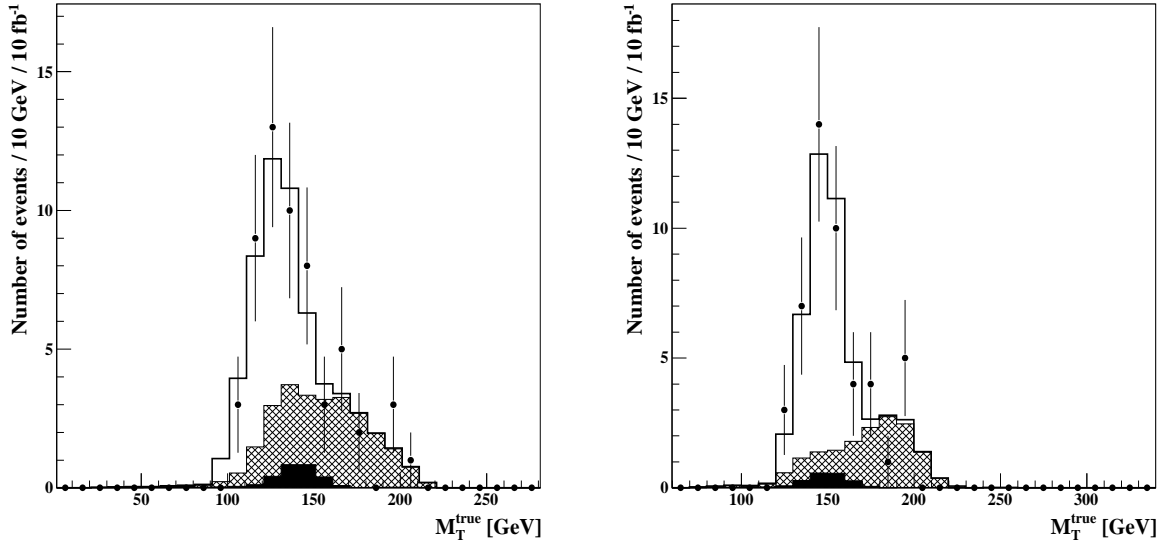


Figure 8: The M_T^{true} distributions for the pseudoexperiment data (dots) and the template (solid line) for $m_H = 140$ (left) and 160 GeV (right) at 10 fb^{-1} luminosity. The lightly and thickly shaded regions represent the $t\bar{t}$ and $WW + 2j$ backgrounds, respectively.

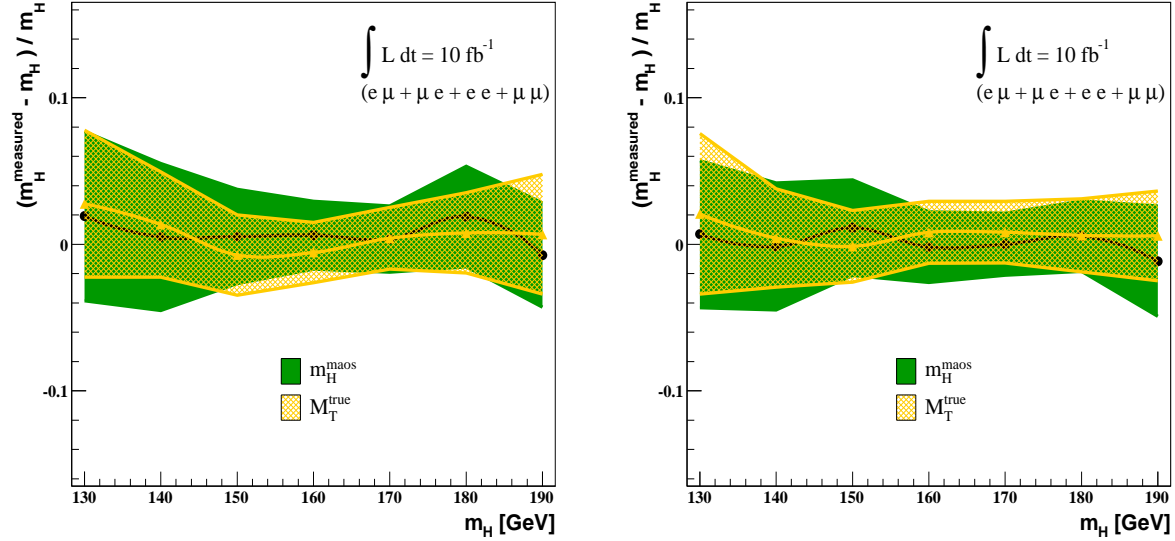


Figure 9: (Left panel) The band showing the $1\text{-}\sigma$ deviation error for the Higgs boson mass determined by the m_H^{maos} and M_T^{true} distributions in the VBF process $qq \rightarrow qqH$ with $H \rightarrow WW^{(*)} \rightarrow l\nu l'\nu'$. The dots and lines denote the Higgs boson mass obtained by the likelihood fit to the pseudoexperiment distributions. (Right panel) The same as in the left frame but without the M_{T2} cuts.

We show our results on the Higgs boson masses and the $1\text{-}\sigma$ errors in the left frame of Fig. 9; these results are obtained using the likelihood fit to the m_H^{maos} and M_T^{true} distributions in the VBF process $qq \rightarrow qqH$ with $H \rightarrow WW^{(*)} \rightarrow l\nu l'\nu'$. We observe that the efficiencies of the two methods are comparable to each other, and both of them provide a good accuracy for the determination of the Higgs mass. Furthermore, to see the role of the M_{T2} cuts in the measurement, we repeat the likelihood fitting of the distributions after applying the same event selection cuts except the M_{T2} cuts; see the right frame of Fig. 9. We find that the final result does not change much since the purity of the event samples is already high enough before imposing the M_{T2} cuts and also the number of signals is relatively smaller than that of the GGF process. Although M_T^{true} and m_H^{maos} have a similar efficiency for the VBF process, we again note that in a situation where there are unknown backgrounds beyond the SM which might smear the endpoint of the M_T^{true} distribution, the m_H^{maos} could be a better choice since the peak is less vulnerable to unknown backgrounds than the endpoint.

5 Conclusions

We performed a comparative study of the Higgs boson mass measurements based on two kinematic observables, M_T^{true} , and m_H^{maos} in dileptonic decays of a W boson pair. For this, we first discussed some features of M_T^{true} and M_{T2} , and also of the MAOS reconstruction of the neutrino momenta in dileptonic W boson decays and the associated invariant mass observable m_H^{maos} . It is found that M_T^{true} and m_H^{maos} can determine the Higgs boson mass in the range $130 \text{ GeV} \leq m_H \leq 190 \text{ GeV}$ with a similar accuracy for both of the two main production mechanisms of the SM Higgs boson at the LHC, i.e. GGF and VBF, up to systematic errors which are not considered in our analysis. Still, it should be noted that the m_H^{maos} distribution has a peak at m_H , while the M_T^{true} distribution has an endpoint, and thus m_H^{maos} can be a better observable when there are some additional backgrounds due to new physics beyond the SM since it is likely that the peak is less vulnerable to unknown backgrounds than the endpoint. One might consider an approach using both m_H^{maos} and M_T^{true} together to extract maximal information on the Higgs boson mass from experimental data. However, our results in Sec. 2 imply that these two variables have a rather strong correlation, and therefore it is not likely that such an approach significantly improves the accuracy of the Higgs mass measurement.

Our study suggests that M_{T2} can be a useful cut variable in the GGF process, as the signal distribution becomes narrower while the background distribution becomes flatter under an M_{T2} cut. Although systematic errors are not considered in our analysis, such behavior of the signal and background distributions might be useful, particularly for reducing various systematic uncertainties in the real analysis of experimental data. In our analysis of the VBF process, M_{T2} is not a particularly useful cut variable compared to others such as the dijet and dilepton invariant masses.

Acknowledgements

We thank W. S. Cho for useful discussions. This work was supported by the KRF Grants funded by the Korean Government (No. KRF-2008-314-C00064 and No. KRF-2007-341-C00010) and the KOSEF Grant funded by the Korean Government (No. 2009-0080844).

References

- [1] G. Aad *et al.* [The ATLAS Collaboration], [arXiv:0901.0512](#).
- [2] G. L. Bayatian *et al.* [CMS Collaboration], *J. Phys. G* **34**, 995 (2007).

- [3] R. Barate *et al.* [The LEP Working Group for Higgs boson searches, ALEPH, DELPHI, L3, and OPAL Collaborations], Phys. Lett. B **565**, 61 (2003) [arXiv:hep-ex/0306033].
- [4] ALEPH, CDF, D0, DELPHI, L3, OPAL, SLD Collaborations, arXiv:0811.4682.
- [5] CDF Collaboration and D0 Collaboration, arXiv:0903.4001; CDF Collaboration and D0 Collaboration, arXiv:0911.3930; The TEVNPH Working Group of the CDF and D0 Collaborations, arXiv:1007.4587.
- [6] M. Spira, Fortsch. Phys. **46**, 203 (1998) [arXiv:hep-ph/9705337].
- [7] For a recent review, see A. Djouadi, Phys. Rept. **457**, 1 (2008) [arXiv:hep-ph/0503172].
- [8] S. Asai *et al.*, Eur. Phys. J. C **32S2**, s19 (2003) [arXiv:hep-ph/0402254].
- [9] C. Ruwiedel, N. Wermes, and M. Schumacher, Eur. Phys. J. C **51**, 385 (2007).
- [10] E. Yazgan *et al.*, Eur. Phys. J. C **53**, 329 (2008) [arXiv:0706.1898].
- [11] V. D. Barger, G. Bhattacharya, T. Han, and B. A. Kniehl, Phys. Rev. D **43**, 779 (1991); M. Dittmar, and H. K. Dreiner, Phys. Rev. D **55**, 167 (1997) [arXiv:hep-ph/9608317].
- [12] W. L. van Neerven, J. A. M. Vermaseren, and K. J. F. Gaemers, NIKHEF-H/82-20; J. Smith, W. L. van Neerven, and J. A. M. Vermaseren, Phys. Rev. Lett. **50**, 1738 (1983); V. D. Barger, A. D. Martin, and R. J. N. Phillips, Z. Phys. C **21**, 99 (1983).
- [13] D. L. Rainwater and D. Zeppenfeld, Phys. Rev. D **60**, 113004 (1999) [Erratum-ibid. D **61**, 099901 (2000)] [arXiv:hep-ph/9906218].
- [14] A. J. Barr, B. Gripaios, and C. G. Lester, JHEP **0907** (2009) 072 [arXiv:0902.4864].
- [15] See S. Dawson and T. Plehn in P. Nath *et al.*, Nucl. Phys. B, Proc. Suppl. **200-202** (2010) 185, [arXiv:1001.2693].
- [16] C. G. Lester and D. J. Summers, Phys. Lett. B **463**, 99 (1999) [arXiv:hep-ph/9906349]; A. Barr, C. Lester, and P. Stephens, J. Phys. G **29**, 2343 (2003) [arXiv:hep-ph/0304226].
- [17] W. S. Cho, K. Choi, Y. G. Kim, and C. B. Park, Phys. Rev. Lett. **100**, 171801 (2008) [arXiv:0709.0288]; B. Gripaios, JHEP **0802** (2008) 053 [arXiv:0709.2740]; A. J. Barr, B. Gripaios, and C. G. Lester, JHEP **0802** (2008) 014 [arXiv:0711.4008]; W. S. Cho, K. Choi, Y. G. Kim, and C. B. Park, JHEP **0802** (2008) 035 [arXiv:0711.4526]; M. M. Nojiri, Y. Shimizu, S. Okada, and K. Kawagoe, JHEP

- 0806** (2008) 035 [[arXiv:0802.2412](https://arxiv.org/abs/0802.2412)]; M. Burns, K. Kong, K. T. Matchev, and M. Park, *JHEP* **0903** (2009) 143 [[arXiv:0810.5576](https://arxiv.org/abs/0810.5576)]; A. J. Barr and C. Gwenlan, *Phys. Rev. D* **80**, 074007 (2009) [[arXiv:0907.2713](https://arxiv.org/abs/0907.2713)].
- [18] K. Choi, S. Choi, J. S. Lee, and C. B. Park, *Phys. Rev. D* **80**, 073010 (2009) [[arXiv:0908.0079](https://arxiv.org/abs/0908.0079)].
- [19] W. S. Cho, K. Choi, Y. G. Kim, and C. B. Park, *Phys. Rev. D* **79** 031701, (2009) [[arXiv:0810.4853](https://arxiv.org/abs/0810.4853)].
- [20] R. K. Ellis, I. Hinchliffe, M. Soldate, and J. J. van der Bij, *Nucl. Phys.* **B297**, 221 (1988).
- [21] J. Conway, <http://www.physics.ucdavis.edu/~conway/research/software/pgs/pgs4-general.htm>
.
- [22] T. Sjostrand, P. Eden, C. Friberg, L. Lonnblad, G. Miu, S. Mrenna, and E. Norrbin, *Comput. Phys. Commun.* **135** (2001) 238 [[arXiv:hep-ph/0010017](https://arxiv.org/abs/hep-ph/0010017)]; T. Sjostrand, S. Mrenna, and P. Skands, *JHEP* **0605** (2006) 026 [[arXiv:hep-ph/0603175](https://arxiv.org/abs/hep-ph/0603175)].
- [23] J. Alwall, P. Demin, S. d. Visscher, R. Frederix, M. Herquet, F. Maltoni, T. Plehn, D. L. Rainwater, and T. Stelzer, *JHEP* **0709** (2007) 028 [[arXiv:0706.2334](https://arxiv.org/abs/0706.2334)].
- [24] C. Amsler *et al.* [Particle Data Group], *Phys. Lett. B* **667**, 1 (2008).